Crystallization under electropulsing suggesting a resonant collective motion of many atoms and modification of thermodynamic parameters in amorphous alloys

Crystallization under electropulsing suggesting a resonant collective motion of many atoms and modification of thermodynamic parameters in amorphous alloys

Hiroshi Mizubayashi,* Natsuki Kameyama, Ting Hao, and Hisanori Tanimoto

Institute of Materials Science, University of Tsukuba, Tsukuba, Ibaraki 305-8573, Japan

For melt-spun amorphous (a-)$Cu_{50}Ti_{50}$ and a-$Pd_{80}Si_{20}$, crystallization under electropulsing was studied by means of the discharge of a condenser with initial current density i_{d0} of the order of 10^9 A/m^2 and decay time τ in between 2 and 0.1 ms, where a specimen was sandwiched by AlN/BN substrates to minimize an effect of joule heating. The crystallization proceeds during electropulsing when i_{d0} is higher than the threshold $i_{d0,c}$. Here $i_{d0,c}$ is a function of τ and shows a minimum value of 1.4×10^9 A/m^2 at $\tau \sim 2$ ms for a-$Cu_{50}Ti_{50}$ and 2.6×10^9 A/m^2 at $\tau \sim 0.9$ ms for a-$Pd_{80}Si_{20}$, where the maximum increase in temperature during electropulsing is about 120 K for a-$Cu_{50}Ti_{50}$ and 50 K for a-$Pd_{80}Si_{20}$, respectively. One-half of the specimen volume crystallizes after a few repetitions of electropulsing with i_{d0} beyond $i_{d0,c}$ for a-$Cu_{50}Ti_{50}$ and after several repetitions for a-$Pd_{80}Si_{20}$. We surmise that for the density fluctuations existing in amorphous alloys, under electropulsing a high-density region undergoes a resonant collective motion as a whole, which induces migrational motions of atoms in the low-density matrix around it. For a-$Pd_{80}Si_{20}$, it is observed that an unknown phase was formed in the early stage of the crystallization under electropulsing and disappeared after further electropulsing. It is also found for a-$Cu_{50}Ti_{50}$ and a-$Pd_{80}Si_{20}$ that for electropulsing with high i_{d0}, the electrical resistivity of a specimen decreased at the early stage of the crystallization and then turned to increase for further electropulsing. These phenomena may be associated with changes in the thermodynamic free energy of phases under an electric current predicted by the theoretical works. We surmise that present electropulsing excites a resonant collective motion of many atoms and modifies the thermodynamic free energy of phases too.

I. INTRODUCTION

The recent review for effects of an electric current on the solid-state phase transformation in metals reports that various significant effects depending on subjects have been found in both crystalline and amorphous metals.[1] For amorphous alloys, a dc electric current of 10^7 A/m^2 causes a decrease in the crystallization temperature by 10–20 K for various melt-spun amorphous (a) alloys.[2–7] Repetition of electropulsing with a duration of 60–100 μs and a peak current density of 10^9 A/m^2 brings about a decrease in the crystallization temperature by 150–170 K for a-Fe-Si-B alloys.[8–12] Both the effects of a dc electric current and repetition of electropulsing may be similar to each other after taking into account difference in the current density and the total time for passing current. The effects are much greater than can be explained by simple electromigration theory and suggest the enhancement of an electromigration effect through a collective motion of many atoms.[1–12] Recent theoretical works on the thermodynamic effect of an electric current on the phase transformation in amorphous alloys report that metastable phases can manifest under influence of an electric current[13,14] or nanocrystalline growth may be a function of the current density.[15] However, present experimental knowledge is very poor for examination of the theoretical works. On the other hand, the probable enhancement of atomic migration associated with a collective motion of many atoms is not taken into account in the theoretical works.

Meanwhile, the peculiar frequency dependence of Young's modulus is found in the frequency range between 10 and 10^3 Hz for a-$Pd_{80}Si_{20}$.[16] It is found that Young's modulus observed in vibrating reed measurements at a strain amplitude of 10^{-6} reveals a deviatory decrease from that observed in quasistatic tensile tests showing a minimum at around 10^2 Hz. On the other hand, it is known that Young's modulus observed in quasistatic tensile tests is lower by 20%–40% for amorphous alloys than for the corresponding crystalline counterparts,[17–20] indicating that the fractional ratio of constituent anelastic strain to the total strain is much larger in amorphous alloys than in the crystalline counterparts. The fractional ratio of constituent anelastic strain is expected to decrease with increasing frequency except when a resonant anelastic process is excited and increases the anelastic strain. Since a decrease in Young's modulus indicates an increase in the fractional ratio of constituent anelastic strain, the peculiar frequency dependence of Young's modulus found for a-$Pd_{80}Si_{20}$ suggests that a certain resonant anelastic process is excited in the frequency range between 10 and 10^3 Hz, mainly at around 10^2 Hz. The decrease in Young's modulus found at around 10^2 Hz is as large as 10%–30%,[16] suggesting that a considerable fraction of atoms in a specimen are associated with the resonant anelastic process. These results may suggest that collective motion of many atoms can be excited as resonant motion as a whole.

Further, the characteristic strain amplitude dependence of Young's modulus is observed at around 10^2 Hz for a-$Pd_{80}Si_{20}$. It is found that Young's modulus observed in vibrating reed measurements at around 10^2 Hz shows a strong increase with increasing strain amplitude, suggesting

that a displacement amplitude of a probable resonant collective motion of many atoms tends to show saturation with increasing strain amplitude.[16] The characteristic strain amplitude dependence of Young's modulus found at around 10^2 Hz is commonly observed for a-$Cu_{50}Ti_{50}$ (Refs. 21 and 22) and a-$Cu_{50}Zr_{50}$ (Ref. 23). Then one can suppose the density fluctuations existing in amorphous alloys where the high-density regions are embedded in the low-density matrix and that migrational motions of atoms in the low-density matrix can be induced when the high-density region undergoes a collective motion as a whole. For such a case, one can expect that enhancement of atomic migration under passing electric current in amorphous alloys is increased when resonant collective motion of many atoms can be excited.

In this case, how to excite such a resonant collective motion of many atoms intensively may be important to pursue experimentally the underlying mechanism for the crystallization of amorphous alloys under the influence of an electric current. After these considerations, we carried out the preliminary works[24,25] for the crystallization of a-$Pd_{80}Si_{20}$ due to electropulsing by means of the discharge of a condenser. The current density i_d during electropulsing decays with increasing elapsed time t as

$$i_d = i_{d0} \exp(-t/\tau), \tag{1}$$

where i_{d0} denotes i_d at the start of electropulsing and τ the decay time of discharge. On the other hand, it is known that a Debye peak shows a maximum at $2\pi f \tau' = 1$, where τ' is the relaxation time of a relaxation process and f a measurement frequency. As a first attempt, we tried electropulsing with τ of the order of 1 ms for a-$Pd_{80}Si_{20}$, where we supposed that the value of τ to excite a resonant collective motion suggested after the peculiar frequency dependence of Young's modulus is the order of $1/(2\pi f)$ with f being the order of 10^2 Hz. In preliminary works, we found that the crystallization of a-$Pd_{80}Si_{20}$ due to electropulsing takes place when i_{d0} is the order of 10^9 A/m², and a maximum temperature attained during electropulsing appears to be much lower than the crystallization temperature observed during the conventional heating measurement. In order to pursue further experimental knowledge, we investigated the crystallization of a-$Pd_{80}Si_{20}$ under electropulsing as well as crystallization under electropulsing in a-$Cu_{50}Ti_{50}$ for which effects of a dc electric current on the crystallization were already reported.[2–5]

II. EXPERIMENT

Amorphous (a-)$Cu_{50}Ti_{50}$ and a-$Pd_{80}Si_{20}$ were prepared as thin tapes by melt spinning in a high-purity Ar gas atmosphere. Specimens were cut out from the amorphous alloy thin tapes. Both surfaces of a specimen were smoothed by polishing mechanically using fine emery paper in water avoiding heat-up during polishing. The thickness and width of specimens after polishing were about 20 μm and 0.8 mm for a-$Cu_{50}Ti_{50}$ specimens and about 25 μm and 0.9 mm for a-$Pd_{80}Si_{20}$ specimens, respectively.

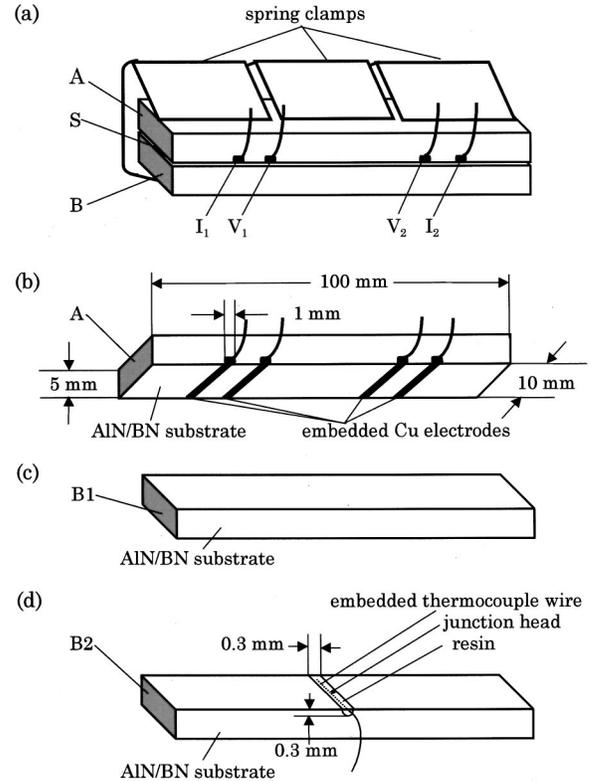Figure 1(a) shows schematic drawing for the specimen setup, where a specimen is sandwiched by two aluminum

FIG. 1. Schematic drawings for (a) the specimen setup, (b) the upper substrate A with embedded copper electrodes, (c) the lower substrate $B1$, and (d) the lower substrate $B2$ with embedded thermocouple wires.

nitride (AlN)/boron nitride (BN) composite substrates and they are fastened as a whole by three spring clamps. It is noted that the thermal conductivity, 90 W/K/m, of the AlN/BN substrates is as high as 83.5 W/K/m of iron. Figure 1(b) is a schematic drawing of the AlN/BN upper substrate A, where four copper electrodes are embedded in the bottom side. The gauge length between current electrodes I_1 and I_2 and that between potential electrodes V_1 and V_2 are 50 and 25 mm for most cases, respectively. Figure 1(c) shows the lower AlN/BN substrate $B1$, which is used for measurements of changes in the resistivity R due to electropulsing. Figure 1(d) shows the lower AlN/BN substrate $B2$, which is used for temperature measurements during electropulsing, where Almel and Chromel thermocouple wires 25 μm in diameter are embedded in the thin channel on the top side. It is noted that the junction head of the thermocouple directly contacts the specimen surface during temperature measurements. In order to ensure good thermal contact between the specimen and AlN/BN substrates, the bottom surface of the upper substrate A and the top surfaces of the lower substrates $B1$ and $B2$ are smoothed by polishing mechanically.

Figure 2 shows the measurement setup for electropulsing which can be made by discharge of a condenser. The decay time τ used in the present work was in between 0.1 and 2.5 ms. The resistivity measurements were conducted by a four-probe method after every electropulsing, where an interval between electropulsings was several minutes. It is noted that the resistivity measurements were made by passing a dc elec-
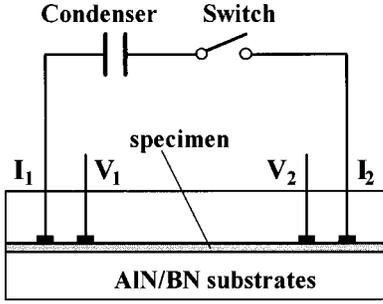
FIG. 2. The measurement setup for electropulsing.

FIG. 3. Resistivity R changes observed for a-$Cu_{50}Ti_{50}$ specimens during constant rate heating in vacuum, where R_0 is R at 300 K in the as-quenched state.

tric current with 10^6 A/m^2 where no influences on the crystallization were expected.[3–6] Separately, measurements of the specimen temperature during electropulsing were carried out, where the thermoelectric power was measured by using a preamplifier and a high-speed analog-to-digital converter.

As already mentioned, i_{d0} and τ in Eq. (1) may be key parameters for the crystallization under electropulsing. We measured changes in R at 300 K after electropulsing, where i_{d0} was increased stepwise. The R/R_0 vs i_{d0} data were compiled for various τ, where R_0 denotes R at 300 K in the as-quenched state. On the other hand, since the electric energy of a pulse given to the unit volume of a specimen, P_d, is indicative of joule heating, the R/R_0 vs P_d plots are also shown after the R/R_0 vs i_{d0} data.

We also carried out resistivity measurements during heating at a constant rate in vacuum by using an electric furnace (furnace heating, hereafter). Thin gold wires were spot-welded to a specimen as current and potential lead wires, and then the specimens with lead wires and thin thermocouple wires were put into a quartz glass tube as a whole. During the furnace heating measurements, the quartz glass tube was evacuated to 10^{-4} Pa, where AlN/BN substrates were not used and electropulsing was not made. For a-$Pd_{80}Si_{20}$, probable effects of rapid heating, magnetic field, and tensile stress on the crystallization process were studied too. The measurement setup for the rapid heating was similar to that of the furnace heating except that light exposure heating was made instead of furnace heating. The measurement setup for furnace heating under tensile stress was similar to that of furnace heating except that a specimen was tensed by a spring through a thin stainless steel wire. The effect of a magnetic field was studied for crystallization under electropulsing, where the measurement setup was similar to Fig. 1(a) except that the AlN/BN substrates A and $B1$ were further sandwiched by permanent magnets.

X-ray diffraction (XRD) measurements were made by the θ-2θ scan using Cu $K\alpha$ radiation, where reflections from Si powder put on a specimen surface were used as reference.

III. RESULTS AND DISCUSSION

A. a-$Cu_{50}Ti_{50}$

Figure 3 shows examples of changes in R observed for a-$Cu_{50}Ti_{50}$ specimens during furnace heating. It is known that a-$Cu_{50}Ti_{50}$ crystallizes to crystalline CuTi (Ref. 26) in one step as seen in Fig. 3. The onset temperature of crystal-
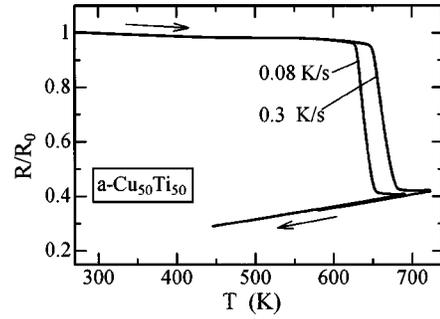
lization, T_x, found in Fig. 3 is 626 K at the heating rate of 0.08 K/s and 646 K at 0.3 K/s, respectively, which show good agreement with T_x reported for a-$Cu_{50}Ti_{50}$ (Ref. 27) after taking into account the difference in the heating rate. The decrease in R at 300 K observed after crystallization, $(\Delta R/R_0)_x$, is -0.8.

Figure 4(a) shows an example of the R/R_0 vs P_d plot observed for an a-$Cu_{50}Ti_{50}$ specimen after electropulsing with $\tau=1.2$ ms, where R/R_0 decreases to about 0.84 in one
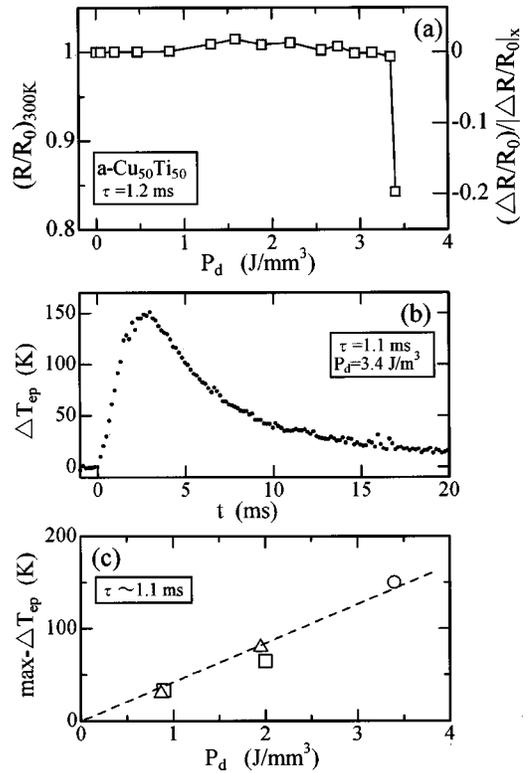

FIG. 4. (a) Changes in R at 300 K observed for an a-$Cu_{50}Ti_{50}$ specimen after electropulsing with $\tau=1.2$ ms, where P_d denotes the electric energy of a pulse given to the unit volume of a specimen. (b) Changes in the specimen temperature, ΔT_{ep}, observed during electropulsing with $\tau=1.1$ ms and $P_d=3.4$ J/mm^3. (c) The maximum increase in the specimen temperature, max-ΔT_{ep}, vs P_d, where the symbols denote the data observed for three specimens. The dashed line is drawn to guide the eyes.
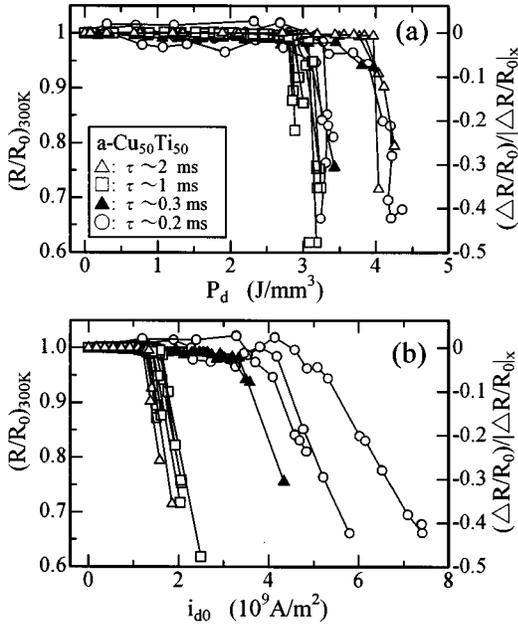
FIG. 5. Changes in R at 300 K observed for a-$Cu_{50}Ti_{50}$ specimens after electropulsing with various τ are plotted against P_d (a) and $i_{d,0}$ (b), respectively. Increased errors for the R/R_0 data observed for the specimens with $\tau \sim 0.2$ ms are due to a decreased gauge length for the R measurements used.

step after electropulsing with $P_d = 3.4$ J/mm^3. Figure 4(b) shows an example of changes in the specimen temperature, ΔT_{ep}, observed during electropulsing with $\tau = 1.1$ ms and $P_d = 3.4$ J/mm^3. After the start of electropulsing, ΔT_{ep} increased rapidly, showing a maximum at about 2.5 ms (max-ΔT_{ep}, hereafter) and then decreased steeply. The max-ΔT_{ep} found is about 150 K for $P_d = 3.4$ J/mm^3, i.e., the maximum specimen temperature attained is about 450 K. Figure 4(c) shows examples of the max-ΔT_{ep} vs P_d data, where max-ΔT_{ep} increases linearly with P_d.

Figure 5(a) is similar to Fig. 4(a), but here the R/R_0 vs P_d data observed for various τ are shown. The threshold value of P_d, $P_{d,c}$, at where R/R_0 starts to show a strong decrease reveals a minimum value of about 2.9 J/mm^3 at $\tau \sim 1$ ms in the present range between 0.2 and 2 ms, indicating that joule heating plays a minor role for the crystallization under electropulsing. It is noted that the max-ΔT_{ep} of about 120 K at P_d of 2.9 J/mm^3 may be found from the max-ΔT_{ep} vs P_d plot shown in Fig. 4(c); i.e., the maximum specimen temperature attained is about 420 K at P_d of 2.9 J/mm^3. Figure 5(b) is a redrawing of Fig. 5(a), but here R/R_0 is plotted against i_{d0}. The threshold value of i_{d0}, $i_{d0,c}$, at where R/R_0 starts to show a strong decrease appears to show a minimum value of about 1.4×10^9 A/m^2 at τ in between 1 and 2 ms, indicating that the decay time of electropulsing plays an important role in crystallization under electropulsing. For a-$Cu_{50}Ti_{50}$ specimens, the maximum decrease in $(\Delta R/R_0)/|\Delta R/R_0|_x$ attained is about -0.5. Such a strong decrease in $(\Delta R/R_0)/|\Delta R/R_0|_x$ took place in a few repetitions of electropulsing with τ of about $1-2$ ms or in several repetitions of electropulsing with τ of about 0.2 ms. It is suggested that intensive atomic migration takes place during electropulsing with i_{d0} beyond
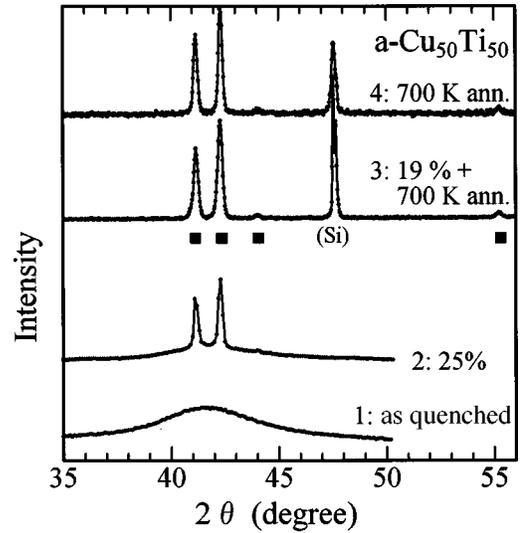
$i_{d0,c}$ and their magnitude is a function of τ. It is noted that an increase in R following a decrease in R due to electropulsing is found at high i_{d0} beyond 7×10^9 A/m^2 for electropulsing with τ of about 0.2 ms. As already mentioned, recent theoretical work on crystallization under electropulsing suggests that nanocrystalline precipitates formed by electropulsing can shrink when the current density is increased beyond a certain threshold value.[15] The increase in R/R_0 observed at high i_{d0} can possibly be explained by the predicted reverse effect of electropulsing at a high current density.

Figure 6 shows the XRD spectra observed for various a-$Cu_{50}Ti_{50}$ specimens. The XRD spectrum 1 observed for the as-quenched state shows a broad XRD peak. The XRD spectrum 4 observed after the furnace heating to 700 K shows good agreement with that expected for crystalline CuTi.[26] The XRD spectrum 2 was observed for the specimen which showed a decrease in R by 25% in R/R_0 due to electropulsing. The XRD spectrum 3 was observed for the specimen which was first subjected to electropulsing with a decrease in R by 19% in R/R_0 and then to the furnace heating to 700 K. The XRD spectrum 2 is composed of the crystalline CuTi XRD peaks and the broad XRD peak from a-$Cu_{50}Ti_{50}$, indicating that the decrease in R due to electropulsing is associated with crystallization. The XRD spectrum 3 is very similar to the XRD spectrum 4 except that the XRD peaks at abound 41.2° and 42.2° in 2θ are broader by about 20% than those seen in the XRD spectrum 4. This result indicates that the mean grain size is smaller in the specimen subjected to electropulsing first than in the specimen subjected to furnace heating alone. In other words, the homogeneous nucleation process can be accelerated under electropulsing.

FIG. 6. XRD spectra observed for various a-$Cu_{50}Ti_{50}$ specimens: 1 = as quenched, 2 = after a 25% decrease in R/R_0 due to electropulsing, 3 = after annealing at 700 K following a 19% decrease in R/R_0 due to electropulsing, and 4 = after annealing at 700 K without electropulsing. The solid symbols denote the XRD spectra expected for crystalline CuTi (Ref. 26). "(Si)" indicated for 3 and 4 is the reflection from Si powder used as reference.

In order to compare the crystallization under electropulsing and the thermally activated crystallization, the time-temperature-transformation (TTT) diagram[28–30] will be visited below. The Johnson-Mehl-Avrami equation[31,32] gives the volume fraction X of crystallization products as (for the case of small X)

$$X \approx (\pi/3)I_\nu u_c^3 t^4, \tag{2}$$

where I_ν denotes the nucleation rate and u_c the crystal growth rate. The homogeneous nucleation rate may be given by[28,29]

$$I_\nu = N_\nu \nu \exp(-Q), \tag{3}$$

where N_ν is the number of single molecules per unit volume and Q is given by

$$Q = \alpha/(T_r^3 \Delta T_r^2). \tag{4}$$

In Eq. (4), T_r is the reduced temperature given by T/T_m and ΔT_r the reduced undercooling denoted by $(T_m \sim T)/T_m$, where T_m denotes the melting temperature. α measures the free energy ΔG^* of forming the critical nucleus, e.g., $\alpha = 1.024$, when one takes $\Delta G^* = 50kT$ at $\Delta T_r = 0.2$.[28,29] In Eq. (3), the frequency factor ν is given by

$$\nu = kT/(3\pi a_0^3 \eta), \tag{5}$$

where a_0 is the mean atomic or ionic diameter for the diffusive jump and the viscosity η may be given by the Fulcher-type equation[33]

$$\eta = A \exp[B/(T - T_0)], \tag{6}$$

where A, B, and T_0 are constants. In Eq. (2), u_c may be given by[28,29]

$$u_c = (\phi D_g/a_0)[1 - \exp(-\Delta T_r \Delta H_{fm}/kT)], \tag{7}$$

where D_g is a diffusion coefficient for atomic motion required for crystal growth, ΔH_{fm} the latent heat of fusion, and ϕ the fraction of sites at the interface where atoms can preferentially be added. The critical cooling rate for glass formation, β_c, approximated for the linear cooling curve required to avoid the nose of the TTT curve for crystallization may be given by[34]

$$\beta_c \approx (T_m - T_n)/t_n, \tag{8}$$

where T_n and t_n are the temperature and time corresponding to the nose of the TTT curve, respectively.

Figure 7 shows the TTT diagram for a-$Cu_{50}Ti_{50}$, where plotted are the incubation time t_x for the crystallization found in isothermal annealing[6] and T_x found during heating at a constant rate γ under the assumption that 20 K/γ corresponds to t_x in isothermal annealing at T_x. In Fig. 7, a redrawing of the T vs t data observed during electropulsing with $P_d = 3.4$ J/mm^3 [see Fig. 4(b)] is shown too. The TTT curve has been estimated as follows. The heat of crystallization of 17.2
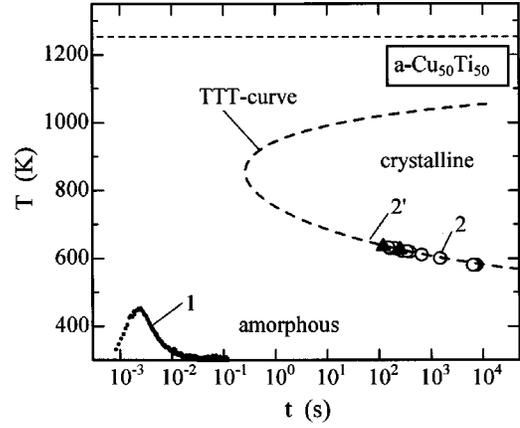

FIG. 7. The TTT diagram for a-$Cu_{50}Ti_{50}$. Curve 1 is a redrawing of the T vs t data shown in Fig. 4(b). The open circles 2 denote the incubation time t_x for crystallization found in isothermal annealing (Ref. 6) and the solid triangles 2$'$ denote T_x found in the constant heating rate (γ) measurements under the assumption of $t_x = 20$ K/γ. The horizontal dashed line denotes T_m. See text for the TTT curve.

kJ/mol reported for a-$Cu_{50}Ti_{50}$ (Ref. 35) is assumed to be ΔH_{fm} in Eq. (7). Here β_c in Eq. (8) is estimated to be about 1600 K/s after the DTA data for a-$Cu_{50}Ti_{50}$ (Ref. 27) and the relationship between β_c and $(T_x - T_g)$ reported,[36] where T_g is the glass transition temperature. A and B in Eq. (6) are assumed to be the same to $A = 3.8 \times 10^{-4}$ Pa s and $B = 1975$ K observed for a-$Pd_{84}Si_{16}$.[37] Here ϕD_g in Eq. (7) is assumed to be $1 \times 10^{-4} \exp(-H_g/kT)[m^2\ s^{-1}]$, where H_g is the activation enthalpy for diffusion. The TTT curve shown in Fig. 7 is found to explain the t_x and T_x data and β_c after assuming $\Delta G^* = 72kT$ at $\Delta T_r = 0.2$ for Eq. (4), $T_0 = 470$ K in Eq. (6), and $H_g = 1.32$ eV, which may be not unreasonable. After the TTT curve and the T vs t data observed during electropulsing, one can say that crystallization under electropulsing cannot be explained by the thermal excitation process alone. This issue will be discussed later on.

B. a-$Pd_{80}Si_{20}$

Figure 8 shows an example of the R vs T data observed for an a-$Pd_{80}Si_{20}$ specimen during furnace heating, where T_x found is about 680 K for a heating rate of 0.2 K/s and $(\Delta R/R_0)_x$ at 300 K is -0.6. The R vs T data are very similar to that reported[38] after taking into a account the difference in
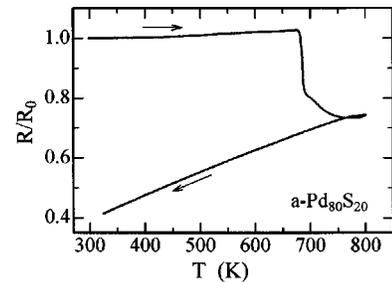

FIG. 8. Resistivity changes observed for an a-$Pd_{80}Si_{20}$ specimen during the furnace heating with the heating rate of about 0.2 K/s.
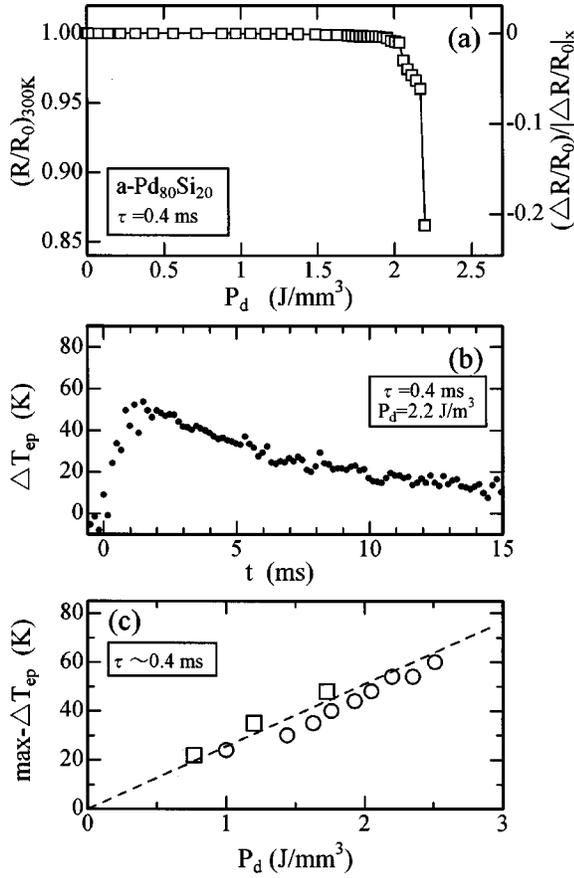
FIG. 9. (a) Changes in R at 300 K observed for an a-Pd$_{80}$Si$_{20}$ specimen after electropulsing with $\tau = 0.4$ ms. (b) Changes in the specimen temperature during electropulsing with $P_d = 2.2$ J/mm^3 and $\tau = 0.4$ ms. (c) The max-ΔT_{ep} vs P_d data, where the symbols denote the data observed for two specimens. The dashed line is drawn to guide the eyes.

the heating rate. Figure 9(a) shows an example of the R/R_0 vs P_d plot observed an a-Pd$_{80}$Si$_{20}$ specimen after electropulsing with $\tau = 0.4$ ms. Figure 9(b) shows an example of changes in the specimen temperature ΔT_{ep} observed during electropulsing with $\tau = 0.4$ ms and $P_d = 2.2$ J/mm^3. After the start of electropulsing, ΔT_{ep} increased rapidly, showing a maximum at about 1.5 ms and then decreased steeply. The max-ΔT_{ep} found is about 50 K for $P_d = 2.2$ J/mm^3, i.e., the maximum specimen temperature attained is about 350 K at P_d of 2.2 J/mm^3. Figure 9(c) shows examples for the max-ΔT_{ep} vs P_d data, where max-ΔT_{ep} increases linearly with P_d in the present experimental range.

Figures 10(a) and 10(b) are similar to Figs. 5(a) and 5(b), but here the R/R_0 vs P_d plot and the R/R_0 vs i_{d0} data observed for various τ observed for a-Pd$_{80}$Si$_{20}$ are shown, respectively. $P_{d,c}$ shows a minimum value of about 2.0 J/mm^3 at $\tau \sim 0.5$ ms in the present τ range between 0.1 and 1.4 ms, indicating that joule heating plays a minor role for crystallization under electropulsing. It is noted that the max-ΔT_{ep} of about 50 K at P_d of 2.0 J/mm^3 may be found from the max-ΔT_{ep} vs P_d plot shown in Fig. 9(c); i.e., the maximum specimen temperature attained is about 350 K at P_d of 2.0 J/mm^3. Here $i_{d0,c}$ is a function of τ and appears to show a
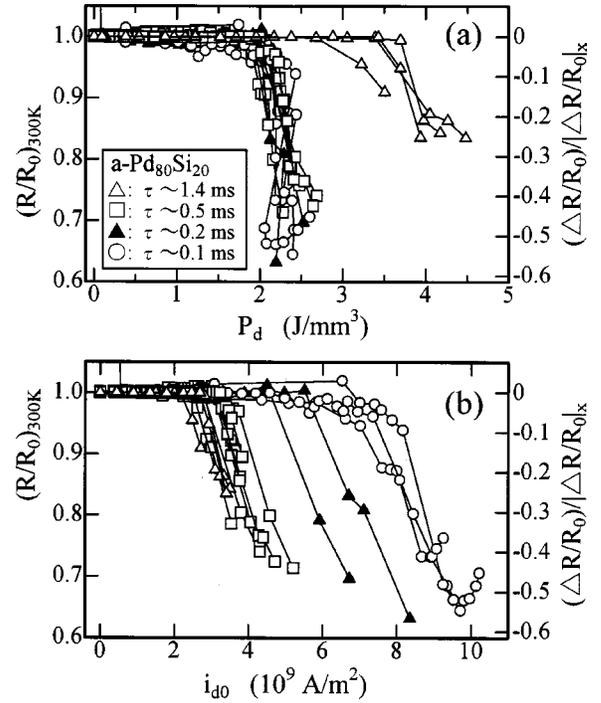

FIG. 10. (a) and (b) are similar to Figs. 5(a) and 5(b), respectively, but here R at 300 K observed for a-Pd$_{80}$Si$_{20}$ specimens is shown. Increased errors for the R/R_0 data observed for the specimens with $\tau \sim 0.1$ ms are due to a decreased gauge length for R measurements used.

minimum value of about 2.6×10^9 A/m^2 at τ between 0.5 and 1.4 ms indicating that the decay time of electropulsing plays an important role on the crystallization under electropulsing. The maximum decrease in $(\Delta R/R_0)/|\Delta R/R_0|_x$ attained after electropulsing is about -0.6 for a-Pd$_{80}$Si$_{20}$ specimens. Such a strong decrease in $(\Delta R/R_0)/|\Delta R/R_0|_x$ takes place in several repetitions of electropulsing, suggesting that intensive atomic migration takes place during electropulsing with i_{d0} beyond $i_{d0,c}$. In Fig. 10(b), it can also be seen that the R/R_0 vs i_{d0} data observed for electropulsing with $\tau \sim 0.1$ ms show an increase in R/R_0 for i_{d0} above about 9×10^9 A/m^2. The increase in R/R_0 observed at high i_{d0} can possibly be explained by the predicted reverse effect of electropulsing at a high current density.[15]

Figure 11 is similar to Fig. 6, but here the XRD spectra observed for a-Pd$_{80}$Si$_{20}$ specimens are shown. The XRD spectrum 1 was observed for the specimen after furnace heating to 800 K. The XRD spectrum 2 was found for the specimen which showed a decrease in R by 6.2% in R/R_0 after electropulsing. The XRD spectra 3–7 were observed for the specimens which were first subjected to electropulsing to various extents for decreases in R and then to furnace heating to 800 K. The XRD spectrum 1 is very similar to that reported.[38–42] The XRD spectrum 2 is composed of the broad XRD peak from an amorphous phase, the XRD peaks being similar to those seen in the XRD spectrum 1 and the unknown XRD peak at about 41° in 2 θ indicated by the vertical arrow in Fig. 11 (the 41° XRD peak). The XRD peaks in the XRD spectrum 2 are much broader than the corre-
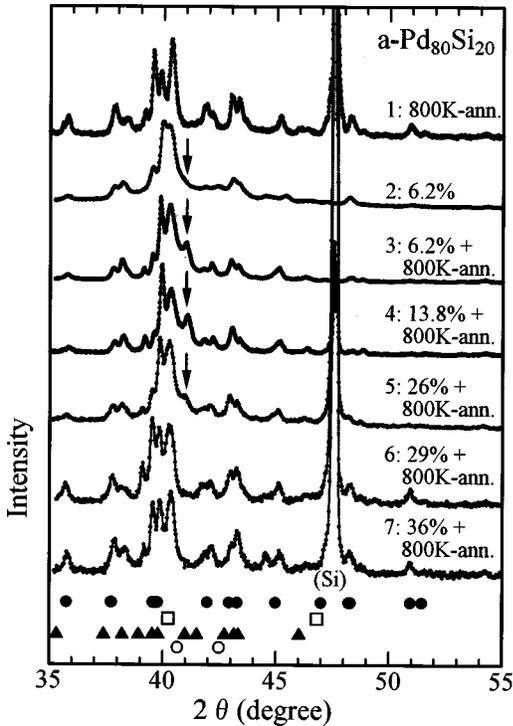
FIG. 11. Similar to Fig. 6, but here the XRD spectra observed in a-$Pd_{80}Si_{20}$ specimens are shown. 1 = after 800 K heat-up without electropulsing. 2 = after a 6.2% decrease in R/R_0 due to electropulsing. 3–7 = after 800 K heat-up without electropulsing following a 6.2%, 13.8%, 26%, 29%, and 36% decrease in R/R_0 due to electropulsing. ● = Pd_3Si (Refs. 38–40). □ = fcc-Pd(Si) (Refs. 38 and 39). ▲ = Pd_9Si_2 (Refs. 41 and 42). ○ = bct-Pd(Si) (Ref. 39). △ = Si(220) from Si powder as reference.
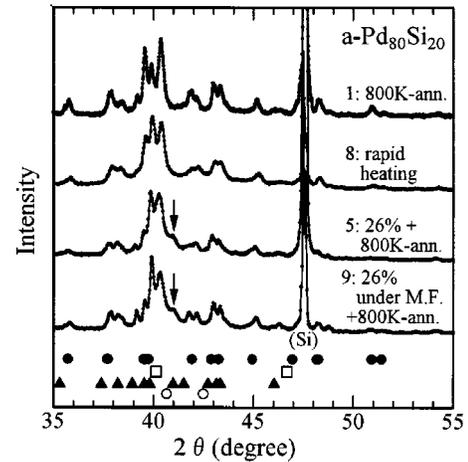

FIG. 12. Similar to Fig. 11. 1 = redrawing of 1 in Fig. 11, 8 = after rapid heating to about 800 K with a heating rate of 130 K/s, 5 = redrawing of 5 in Fig. 11, and 9 = after furnace heating to 800 K following electropulsing under a magnetic field of about 0.5 T.

sponding XRD peaks in the XRD spectrum 1, indicating that the size of crystallites is much smaller for crystallization due to electropulsing than for crystallization attained during furnace heating to 800 K. For the XRD spectrum 3 which was observed after furnace heating to 800 K following the XRD spectrum 2, the XRD peaks became to be sharper than those found in the XRD spectrum 2, but were broader than those observed in the XRD spectrum 1, suggesting that the homogeneous nucleation process is enhanced by electropulsing. The 41° XRD peak became stronger in the XRD spectrum 3 than in the XRD spectrum 2, suggesting that the unknown phase responsible for the 41° XRD peak is stable below 800 K. On the other hand, the XRD spectra 4–7 indicate that the unknown phase formed in the early stage of crystallization due to electropulsing disappears after further electropulsing.

In a-$Pd_{80}Si_{20}$, the unknown phase found in the early stage of crystallization due to electropulsing may be a probe to study probable effects of rapid heating and magnetic field by which electropulsing is accompanied. In Fig. 12, the XRD spectra 1 and 5 are redrawings of the XRD spectra 1 and 5 in Fig. 11, respectively. The XRD spectrum 8 was observed for the specimen subjected to rapid heating to about 800 K with a heating rate of 130 K/s by means of light exposure, where electropulsing was not made. The specimen for the XRD spectrum 9 was first subjected to electropulsing in a magnetic field of about 0.5 T, where R decreased by 26% after electropulsing, and then to furnace heating to 800 K. The XRD spectrum 8 is very similar to the XRD spectrum T except that the XRD peaks are broader in the XRD spectrum 8 than in the XRD spectrum 1, suggesting that the mean grain size of crystallites is smaller after rapid heating than after furnace heating. The 41° XRD peak was not detected for the XRD spectrum 8. The XRD spectrum 9 is very similar to the XRD spectrum 5 suggesting that the magnetic field associated with electropulsing is not responsible for the manifestation of the unknown phase formed in the early stage of crystallization due to electropulsing.

Recently, it has been found that an electric current may induce internal stress in amorphous alloys.[6,43,44] On the other hand, it is reported that the incubation time for crystallization of a-$Pd_{80}Si_{20}$ to the metastable solid solution (SS) becomes shorter under a tensile stress of about 400 MPa, where isothermal annealing has been made in the temperature range between 520 and 400 K.[45,46] However, no reports are found for a probable effect of tensile stress on the crystallization of a-$Pd_{80}Si_{20}$ to the stable phases (see Figs. 8 and 11), which may be accelerated by electropulsing. Then we carried out furnace heating measurements under tensile stress, where electropulsing was not made. Figure 13 shows changes in R observed for the a-$Pd_{80}Si_{20}$ specimens during furnace heating with a heating rate of 0.4 K/s under various tensile stresses below 522 MPa. All specimens showed an increase in R due to creep deformation and failed at around 650 K. Since the specimen was tensed by a spring, one-half of the specimen was pulled out from the furnace region immediately after its failure. No crystallization was detected by the XRD measurement of the pulled-out specimen (not shown here), indicating that the lower bound of the crystallization of a-$Pd_{80}Si_{20}$ to stable phases under a tensile stress of 522 MPa is about 650 K for a heating rate of 0.4 K/s.

Figure 14 shows the TTT diagram of a-$Pd_{80}Si_{20}$ reported.[38,39,45,46] In Fig. 14, the symbols 2 denote T_x found in the present constant heating rate (γ) measurements, where we assume that 20 K/γ corresponds to t_x for isothermal an-
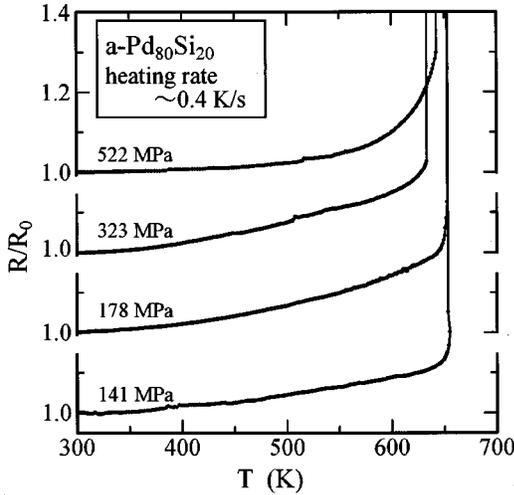
FIG. 13. Changes in R observed for a-$Pd_{80}Si_{20}$ specimens under various tensile stresses during furnace heating with heating rate of 0.4 K/s, where no electropulsing was given.

nealing at T_x after the isothermal annealing data reported. The dashed line $2'$ denotes the lower bound of the crystallization of a-$Pd_{80}Si_{20}$ to stable phases under a tensile stress of about 500 MPa, where $t_x = 20 \, K/\gamma$ is assumed. The T vs t data 1 are a redrawing of Fig. 9(b). The TTT curve has been estimated as follows: The heat of crystallization of 467 J/mol reported for a-$Pd_{84}Si_{16}$ (Ref. 37) is assumed to be ΔH_{fm} in Eq. (7). Here β_c in Eq. (8) is assumed to be 2500 K/s reported for a-$Pd_{84}Si_{16}$.[47] A and B in Eq. (6) are assumed to be the same to $A = 3.8 \times 10^{-4}$ Pa s and $B = 1975$ K observed for a-$Pd_{84}Si_{16}$.[37] Here ϕD_g in Eq. (7) is assumed to be 1 $\times 10^{-4} \exp(-H_g/kT)[m^2 \, s^{-1}]$. The TTT curve shown in Fig. 14 is found to explain the t_x and T_x data and β_c after assuming $\Delta G^* = 25kT$ at $\Delta T_r = 0.2$ for Eq. (4), $T_0 = 551$ K in Eq.
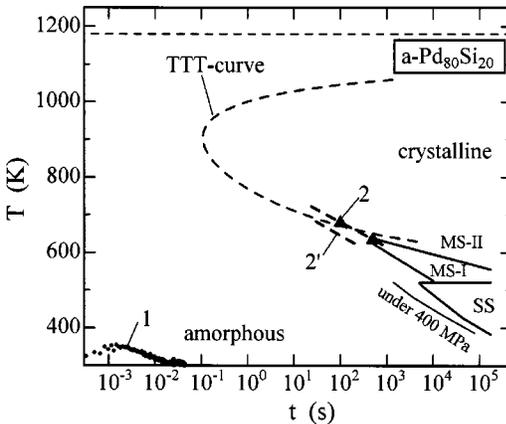

FIG. 14. The temperature-time-transformation diagram of a-$Pd_{80}Si_{20}$ reported (Refs. 38, 39, 45, and 46). SS: a metastable solid solution with fcc structure. MS-I: the appearance of crystallites with fcc structure in the amorphous structure. MS-II: the formation of a complex ordered metastable phase in the amorphous matrix with dispersed MS-I phase. The dashed curve: the onset temperature for SS under tensile stress of about 400 MPa. The T vs t curve 1, the solid triangles 2, the dashed line 2, and the TTT curve are the present data. See text for details.
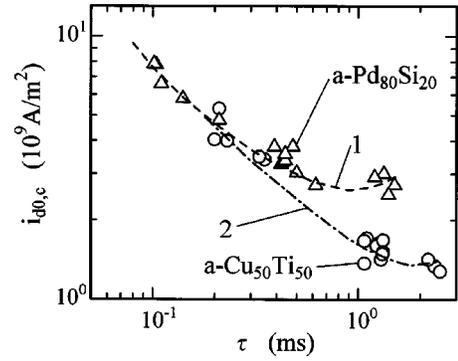

FIG. 15. The threshold current density $i_{d0,c}$ found for a-$Pd_{80}Si_{20}$ and a-$Cu_{50}Ti_{50}$ specimens is plotted against the decay time τ for electropulsing.

(6), and $H_g = 1.84$ eV. After the TTT curve and the T vs t data observed during electropulsing, one can say that crystallization under electropulsing cannot be explained by the thermal excitation process alone as well as that in a-$Cu_{50}Ti_{50}$.

C. Crystallization under electropulsing

The R/R_0 vs P_d data shown in Figs. 5(a) and 10(a) indicate that $P_{d,c}$ is function of τ, suggesting that joule heating plays a minor role on crystallization under electropulsing. The max-ΔT_{ep} vs t data shown in Figs. 4(c) and 9(c) indicate that the maximum temperature attained during electropulsing with τ of the order of 1 ms at the onset of crystallization is about 420 K for a-$Cu_{50}Ti_{50}$ and about 350 K for a-$Pd_{80}Si_{20}$, respectively. It is suggested that crystallization under electropulsing cannot be explained by the thermal activation process alone for both a-$Cu_{50}Ti_{50}$ and a-$Pd_{80}Si_{20}$.

After the $(R/R_0)_{300 \, K}$ vs i_{d0} data shown in Figs. 5(b) and 10(b), we defined the threshold $i_{d0,c}$ for crystallization under electropulsing as i_{d0} found at $(R/R_0)_{300 \, K} = 0.95$. In Fig. 15, $i_{d0,c}$ is plotted against τ. As already mentioned, $i_{d0,c}$ is a function of τ, where $i_{d0,c}$ appears to show a minimum value of 1.4×10^9 A/m^2 at $\tau \sim 2$ ms for a-$Cu_{50}Ti_{50}$ and 2.6 $\times 10^9$ A/m^2, at $\tau \sim 0.9$ ms for a-$Pd_{80}Si_{20}$, respectively. This result may support the idea of density fluctuations existing in amorphous alloys mentioned above: i.e., under electropulsing, a high, density region undergoes a resonant collective motion as a whole which induces migrational motions of atoms in the low-density matrix around it. The assumption that the resonant frequency f' of collective motion is the order of $1/(2\pi\tau)$ may give f' of the order of 10^2 Hz for $\tau \sim 2$ ms for a-$Cu_{50}Ti_{50}$ and $\tau \sim 0.9$ ms for a-$Pd_{80}Si_{20}$. It is noted that f' of the order of 10^2 Hz shows good agreement with the measurement frequency f of the order of 10^2 Hz at where resonant collective motion of many atoms may be excited by means of elastic vibrations.[16]

On the other hand, Lai *et al.*[8,12] report that repetition of electropulsing with a peak current density of 10^9 A/m^2 causes the lowering of T_x by 150–170 K and nanocrystallization of a-Fe-Si-B alloys. The effects of electropulsing on crystallization found by them are, qualitatively, very similar to the present results. As already mentioned, however, the

enhancement of crystallization found by Lai *et al.* may fall in the range which can be found after extrapolation from the enhancement of crystallization observed under a passing dc electric current of 10^7 A/m^2.[3–6] On the other hand, the crystallization under the present electropulsing appears to be out of this range. Such a different effect found between the electropulsing employed by Lai *et al.*[8,12] and the present electropulsing may be associated with the effective frequency of electropulsing. The effective frequency f' of electropulsing employed by Lai *et al.* is between 5 and 8 kHz,[48] which corresponds to τ of 0.02–0.03 ms in the present electropulsing after assuming the relationship of $f' = 1/(2\pi\tau)$. The extrapolation of the $i_{d0,c}$ vs τ data shown in Fig. 15 gives $i_{d0,c} \sim 10^{11}$ A/m^2 at τ of 0.02–0.03 ms, which is two decades larger than the peak current density of 10^9 A/m^2 of electropulsing employed by Lai *et al.*[8,12]

As mentioned for Figs. 5(a) and 10(a), the decrease in $(\Delta R/R_0)/|\Delta R/R_0|_x$ attained after electropulsing is as large as -0.5 and -0.6 for a-Cu$_{50}$Ti$_{50}$ and a-Pd$_{80}$Si$_{20}$ specimens, respectively, suggesting that both the nucleation and growth processes are enhanced under present electropulsing. In other words, atomic migration intensively proceeds during electropulsing for τ of the order of 1 ms below 420 K in a-Cu$_{50}$Ti$_{50}$ and below 350 K in a-Pd$_{80}$Si$_{20}$. On the other hand, for the nature of the inhomogeneities existing in a computer-built model amorphous metal, it is reported that the geometrical coordination numbers extend over several atomic distances and the spatial fluctuations of the shear modulus and atomic volume are quite variable.[49] After a shear deformation, the displacement map of atoms shows significant displacements of most atoms in localized regions (the free-volume-rich regions, hereafter) and no displacements in the remaining regions (the free-volume-poor regions, hereafter).[49] We speculate that the present electropulsing excites a collective motion of the free-volume-poor regions as a whole, which brings about migrational motions of most atoms in the free-volume-rich regions. In this case, nucleation and growth are expected to proceed in the free-volume-rich regions. The influence of electric current on the elastic properties found for amorphous alloys suggests that the number of atoms involved in the collective motion of one free-volume-poor region is 10^3–10^4.[6,43] On the other hand, the number of atoms for one free-volume-poor region in the model amorphous metal[49] is 10^2–10^3, which may not be so different from the value mentioned above after taking in account that the number of atoms for the model calculation is very limited. On the other hand, the excitation of intensive migrational motions of atoms in the free-volume-rich region may correspond to an increase in local temperature in the free-volume-rich region. However, the TTT diagrams shown in Figs. 7 and 14 indicate that no crystallization is expected for $\tau \sim 1$ ms in a-Cu$_{50}$Ti$_{50}$ or for $\tau \sim 0.5$ ms in a-Pd$_{80}$Si$_{20}$, suggesting that a further unknown dynamic process is involved for crystallization under electropulsing.

For a-Pd$_{80}$Si$_{20}$, an unknown phase is formed in the early stage of crystallization due to electropulsing and it disappears in the later stage (see Fig. 11). On the other hand, no new phases are observed after crystallization of a-Cu$_{50}$Ti$_{50}$ under electropulsing (see Fig. 6). As already mentioned, re-cent theoretical works for the effects of an electric current on the crystallization in amorphous alloys report that metastable phases can manifest under the influence of an electric current.[13,14] No observation of new phases after crystallization of a-Cu$_{50}$Ti$_{50}$ under electropulsing may reflect that a-Cu$_{50}$Ti$_{50}$ always crystallizes to c-CuTi, suggesting that the thermodynamic free energy of c-CuTi is lower than that of probable metastable crystalline phases under passing electric current in the present current densities. In contrast, various metastable phases have been reported for the crystallization of a-Pd$_{80}$Si$_{20}$,[38,39,42,45,46] suggesting that the difference of the thermodynamic free energy of metastable phases can be modified under an electric current in the present current densities.

For both a-Cu$_{50}$Ti$_{50}$ [Fig. 5(b)] and a-Pd$_{80}$Si$_{20}$ [Fig. 10(b)], an increase in R following a decrease in R due to electropulsing is observed at high i_{d0}. As already mentioned, this phenomenon may also be explained by the thermodynamic effect of an electric current on the crystallization, where it is suggested that nanocrystalline precipitates formed by electropulsing can shrink when the current density is increased beyond a certain threshold value.[15]

IV. CONCLUSION

For a-Cu$_{50}$Ti$_{50}$ and a-Pd$_{80}$Si$_{20}$, crystallization under electropulsing was studied by means of the discharge of a condenser with τ of 2–0.1 ms. Crystallization proceeds during electropulsing with i_{d0} beyond the threshold $i_{d0,c}$, where $i_{d0,c}$ is a function of τ and shows a minimum value of 1.4 $\times 10^9$ A/m^2 at $\tau \sim 2$ ms for a-Cu$_{50}$Ti$_{50}$ and 2.6×10^9 A/m^2 at $\tau \sim 0.9$ ms for a-Pd$_{80}$Si$_{20}$, respectively. The maximum temperature attained during electropulsing is about 420 K for a-Cu$_{50}$Ti$_{50}$ and about 350 K for a-Pd$_{80}$Si$_{20}$, respectively, suggesting that the crystallization under electropulsing cannot be explained by thermal activation process alone. One-half of the specimen volume crystallized after a few repetitions of electropulsing with i_{d0} beyond $i_{d0,c}$ for a-Cu$_{50}$Ti$_{50}$ and after several repetitions for a-Pd$_{80}$Si$_{20}$, indicating that intensive atomic migration proceeded during electropulsing for the order of 1 ms. We surmise that for the density fluctuations existing in amorphous alloys, under electropulsing, a high-density region undergoes resonant collective motion as a whole which induces migrational motions of atoms in the low-density matrix around it. For a-Pd$_{80}$Si$_{20}$, the unknown phase is formed in the early stage of the crystallization due to electropulsing and it disappears in the later stage. On the other hand, no new phases are observed after crystallization of a-Cu$_{50}$Ti$_{50}$ under electropulsing. These phenomena may be explained by a change in the thermodynamic free energy of phases by an electric current predicted in the recent theoretical works. For a-Cu$_{50}$Ti$_{50}$ and a-Pd$_{80}$Si$_{20}$, it is also found that for electropulsing with high i_{d0}, the electrical resistivity of the specimen decreases at an early stage of the crystallization and increased for further electropulsing. Observations of an unknown phase and the reverse effect at high $i_{d0,c}$ may also be associated with the thermodynamic effects of electropulsing predicted by the theoretical works. We surmise that present electropulsing excites resonant collective motion of

the free-volume-poor regions which causes migrational atomic motions in the free-volume-rich regions around them. In addition, the thermodynamic effects of an electric current may also be involved for crystallization under the present electropulsing.

*Electronic address: mizuh@ims.tsukuba.ac.jp

[1] H. Conrad, Mater. Sci. Eng., A **287**, 227 (2000).

[2] H. Mizubayashi and S. Okuda, Phys. Rev. B **40**, 8057 (1989).

[3] H. Mizubayashi and R. Takemoto, Defect Diffus. Forum **95−98**, 1187 (1993).

[4] R. Takemoto and H. Mizubayashi, Mater. Sci. Eng., A **179/180**, 275 (1994).

[5] R. Takemoto and H. Mizubayashi, Acta Metall. Mater. **43**, 1495 (1995).

[6] R. Takemoto, M. Nagata, and H. Mizubayashi, Acta Metall. Mater. **44**, 2787 (1996).

[7] Y. Onodera, J. Phys.: Condens. Matter **7**, 1235 (1995).

[8] Z. H. Lai, H. Conrad, Y. S. Chao, S. Q. Wang, and J. Sun, Scr. Metall. **23**, 305 (1989).

[9] Z. H. Lai, Y. S. Chao, H. Conrad, and K. Chu, J. Mater. Res. **10**, 900 (1995).

[10] G.-Q. Teng, Y. Chao, Z.-H. Lai, and L. Dong, Phys. Status Solidi A **156**, 265 (1996).

[11] G.-Q. Teng, Y. Chao, L. Dong, Y. Geng, and Z. Lai, Jpn. J. Appl. Phys., Part 1 **35**, 5320 (1996).

[12] Z. H. Lai, H. Conrad, G. Q. Teng, and Y. S. Chao, Mater. Sci. Eng., A **287**, 238 (2000).

[13] Y. Dolinsky and T. Elperin, Phys. Rev. B **58**, 3008 (1998).

[14] Y. Dolinsky and T. Elperin, Mater. Sci. Eng., A **278**, 219 (2000).

[15] R. S. Qin, S. X. Su, J. D. Guo, G. H. He, and B. L. Zhou, Nanostruct. Mater. **10**, 71 (1998).

[16] H. Mizubayashi, T. Okamoto, K. Koyama, and M. Horiuchi, Acta Mater. **46**, 1257 (1998).

[17] S. Jovanovic and C. S. Smith, J. Appl. Phys. **32**, 121 (1961).

[18] M. F. Ashby, A. N. Nelson, and R. M. A. Centamore, Scr. Metall. **4**, 715 (1970).

[19] D. Weaire, M. F. Ashby, J. Logan, and M. J. Weins, Acta Metall. **19**, 779 (1971).

[20] H. S. Chen, J. Appl. Phys. **49**, 3289 (1978).

[21] H. Mizubayashi, S. Okuda, and Y. Ikeda, Phys. Status Solidi A **116**, 633 (1989).

[22] H. Mizubayashi, S. Hoshina, and S. Okuda, J. Non-Cryst. Solids **117/118**, 203 (1990).

[23] H. Mizubayashi, M. Kaida, S. Otsuka, and S. Okuda, Acta Metall. Mater. **42**, 2099 (1994).

[24] H. Mizubayashi and N. Kameyama, in *Proceedings of the Third Pacific Rim International Conference on Advanced Materials and Processing*, edited by M. A. Imam *et al.* (Minerals, Metals and Materials Society, Warrendale, PA, 1998), p. 2057.

[25] H. Mizubayashi and N. Kameyama, in *Proceedings of the International Conference on Solid State Phase Transformations*, edited by M. Koiwa *et al.* (Japan Institute of Metals, Sendai, 1999), p. 1235.

[26] R. C. Bowman, Jr., A. J. Maeland, and W.-K. Rhim, Phys. Rev. B **26**, 6362 (1982).

[27] R. A. Dunlap and K. Dini, J. Phys. F: Met. Phys. **14**, 2797 (1984).

[28] D. R. Uhlmann, Mater. Sci. Res. **4**, 172 (1969).

[29] P. I. K. Onorato and D. R. Uhlmann, J. Non-Cryst. Solids **22**, 367 (1976).

[30] N. Nishiyama and A. Inoue, Acta Mater. **47**, 1487 (1999).

[31] W. A. Johnson and R. F. Mehl, Trans. AIME **135**, 416 (1939).

[32] M. Avrami, J. Chem. Phys. **7**, 1103 (1939).

[33] G. S. Fulcher, J. Am. Ceram. Soc. **6**, 339 (1925).

[34] H. A. Davies, Phys. Chem. Glasses **17**, 159 (1976).

[35] R. C. Bowman, Jr., R. J. Furlan, J. S. Cantrell, and A. J. Maeland, J. Appl. Phys. **56**, 3362 (1984).

[36] A. Inoue, Acta Mater. **48**, 279 (2000).

[37] Y. Nishi, N. Kayama, S. Kiuchi, K. Sizuki, and T. Masumoto, J. Jpn. Inst. Met. **44**, 1336 (1980).

[38] T. Masumoto and R. Maddin, Acta Metall. **19**, 725 (1971).

[39] H. Iwasaki and T. Masumoto, J. Mater. Sci. **13**, 2171 (1978).

[40] B. Aronsson and A. Nylund, Acta Chem. Scand. **14**, 1011 (1960).

[41] J. A. Wysocki and P. E. Duwez, Metall. Trans. A **12**, 1455 (1981).

[42] Z. Li, Y. Qin, and Y. He, Phys. Status Solidi A **148**, 351 (1995).

[43] H. Mizubayashi and R. Takemoto, J. Alloys Compd. **211/212**, 340 (1994).

[44] H. Mizubayashi and T. Okamoto, Mater. Sci. Forum **304−306**, 355 (1999).

[45] R. Maddin and T. Masumoto, Mater. Sci. Eng. **9**, 153 (1972).

[46] T. Masumoto and R. Maddin, Mater. Sci. Eng. **19**, 1 (1975).

[47] A. Inoue, Mater. Trans., JIM **36**, 866 (1995).

[48] A. F. Sprecher, S. L. Mannan, and H. Conrad, Acta Metall. **34**, 1145 (1986).

[49] K. Maeda and S. Takeuchi, J. Phys. F: Met. Phys. **12**, 2767 (1982).